**Proceedings of the
International Conference on Power Engineering-09
(ICOPE-09) November 16-20, 2009, Kobe, Japan**

Heat and Reaction Characteristics of Multistage Alcoholic-Fuel Reformer (2nd Report: Velocity and Radical Chemiluminescence Measurements)

Yasuhiro RAI[1], Kazuya TATSUMI[1,2], Keisuke KUWABARA[1] and Kazuyoshi NAKABE[1,2]

1. Dept. of Mech. Eng. and Sci., Kyoto University, Yoshida-Honmachi, Sakyo-ku, Kyoto 606-8501, Japan
2. Adv. Research Inst. Fluid Sci. and Eng., Kyoto University

ABSTRACT The present study discusses the heat and reaction characteristics of the multistage alcoholic-fuel reformer. Gas temperatures, exhaust gas components and radical chemiluminescence intensities were monitored in the reformer. In the single-stage case, temperature level inside the reactor and decomposition ratio of CH_3OH, α, were decreased with an increase in equivalence ratio, ϕ ($\geq$3.0). In contrast, higher ϕ resulted in lower OH-radical chemiluminescence intensity inside the reactor. In the double-stage case that a portion of the air was supplied to the secondary port, a slight increase in the H_2 concentration was observed, and an excessive increase of local temperature was avoided. These results show the double-stage air supply is effective to control the temperature distribution and avoid an undesired hot-spot in the reformer without causing a significant change in the components of the product gas.

Keywords: Compact fuel reformer, Hydrogen production, Multistage reactor, Temperature measurement, Chemiluminescence intensity measurement

1. INTRODUCTION

Hydrogen, which is called one of the most promising energy sources, can be used for highly efficient energy systems such as fuel cells and hydrogen engines. Although large-scale industrial process of hydrogen production has been established in chemical plants, time is required until the infrastructures of hydrogen distributions and storages are introduced into the society. Meanwhile, on-site hydrogen production is essential for future distributed power supplying systems. A multistage compact fuel reformer, which is composed of multiple ports for step-by-step supply of reactants, air, and water vapor, was applied to produce hydrogen from alcoholic fuels and examined in terms of heat and reaction characteristics. Reactants were supplied partially to the reformer from several ports in order to perform effective and quick control of local heat balance and temperature inside the reformer, which is believed to result in the enhancement of reforming effectiveness and the reduction of undesired exhausts such as soot or CO [1-5].

In this paper, results of a prototype multistage tube type reformer are reported. Methanol was used as fuel in the both previous and present experiments [5]. Alcoholic fuel is relatively easy to transport and store since it is chemically stable and is in liquid phase under normal temperature and pressure. It is, therefore, considered to be suitable for compact energy supply systems with an output of several kilo watts [6]. No catalyst was applied to the reformer in the studies. It is reported that the thermal condition of the reformer greatly affects the reforming performance in either case: with and without catalyst [7, 8]. Therefore, as the initial step of evaluating the multistage reformer, the experiment was conducted without inserting the catalyst to discern the degree of effects of multiplying the reaction stages from those of the catalyst characteristics.

Reforming gas temperatures, exhaust gas components, and radical chemiluminescence intensities were monitored in the reformer. OH-radical chemiluminescence is measured to evaluate the occurrence of the gas reaction. Flow characteristic inside the reactor was evaluated by LDV measurement inside the acrylic pipe of the same dimensions as the reformer. The effects of equivalence ratio and reactant flow rate on the reforming characteristics are discussed, mainly focusing on the partial oxidation reaction (POR).

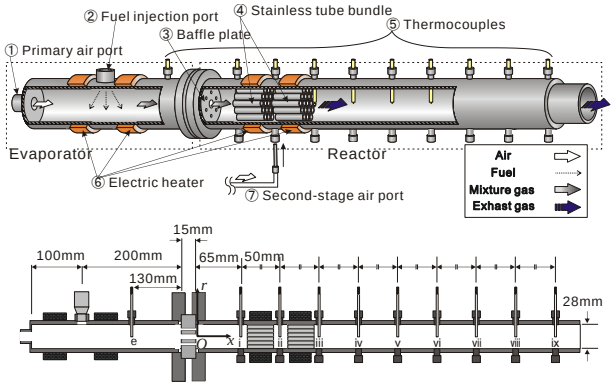

Fig. 1. Schematic view of the reformer (evaporator & reactor).

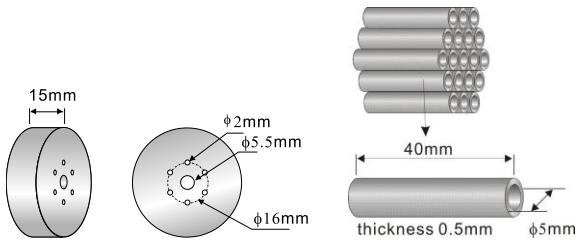

(a) Baffle plate (b) Tube bundle

Fig. 2. Elements of the reformer.

2. EXPERIMENTAL SETUP

Figure 1 illustrates the schematic and cross-sectional views of the reformer. As shown in the figure, the reformer

was composed of two parts, i.e., the evaporator and reactor.

The evaporator was made of a galvanized steel pipe with inner diameter and length of 28mm and 200mm, respectively. A fuel supply port was located at the side surface of the evaporator, on which an injector with electric valve was mounted. An electrical rectangular signal was sent from a function generator (Yokogawa; WE500, WE7281) to this injector to control the valve opening. Therefore, flow rate of the fuel jet was controlled by adjusting the frequency and duty ratio of the signal to a certain value. An air supply port was set at the upstream end of the evaporator. Air supplied to this port was provided from a compressor, and the flow rate was controlled by rotameter and valve (Kofloc; RK1250). In the upstream and downstream areas adjacent to the fuel supply port, electric band heaters (Sakaguchi E.H. Voc.; BH3430) were wrapped around the evaporator pipe. This heater, powered by a voltage slider (Yamabishi; V-130-3), raised the temperature of the evaporator wall up to specified °C. Thus, the fuel which is injected from the fuel supply port, impinged on the inner wall of the evaporator, and was vaporized there. The vaporized fuel mixing with the air flowing from the upstream air supply port, was then supplied to the reactor through a baffle plate.

As shown in Fig. 1, this baffle plate was located between the evaporator and reactor. Multiple holes were drilled in the 12mm-thick stainless disk. The configuration of the holes is shown in Fig. 2(a), i.e., a 5.5mm-hole was located at the center of the disk and six holes with 2mm diameter surrounded the center one. This multi-hole baffle plate was expected to enhance the mixing between the vaporized fuel and air, and to prevent backfire from the reactor to the evaporator.

The reactor was made of a stainless steel pipe 28mm in diameter and 500mm in length. In the areas of $70 \le x \le 110$mm and $120 \le x \le 160$mm, bundles of 19 stainless tubes (each tube inner diameter = 4mm, length = 40mm; see Fig. 2(b)) were inserted in the reactor. These tube bundles were expected to enhance the reaction efficiency and also maintain a stable reaction under high equivalence ratio by increasing the heat transfer at the tube walls. Band heaters (Watlow; MB01E1AB3005) were attached to the pipe sidewall at each location identical to where the tube bundles were inserted. These heaters were powered by a voltage slider in the same way as those in the evaporator, and the pipe wall was preheated before the experiment started.

Several loading ports were applied to the sidewalls of the evaporator and reactor at the locations shown in Fig. 1. Probes for temperature measurement made of K type thermocouples were inserted into the pipe through these ports. This probe was a two-hole ceramic tube (tube outer diameter = 3mm) having the weld spot of the thermocouple wires exposed at the tip. To protect the exposed parts of the thermocouples from the flame and reactive gas, and also to prevent any catalysis effects, the thermocouples were coated by silica-particles generated by burning the town gas into which Hexamethyldisiloxane was mixed. The signals from the thermocouples were recorded by a personal computer through a digital multi-thermometer (Keyence; NR-1000). The sampling rate and accuracy of the temperature measurement was 1s and ±1°C, respectively.

Additional air was also supplied through these ports to the reactor operated in the way of multistage reforming. The end of the air-feed tube was located at the central axis

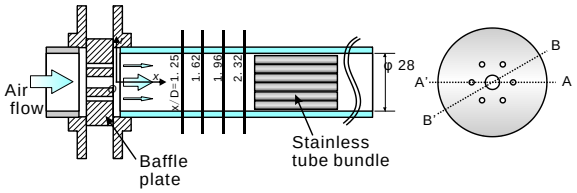

Fig. 3. Cross-sectional view of the LDV velocity measurement points.

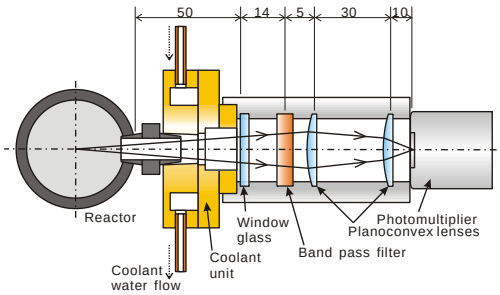

Fig. 4 Cross-sectional view of the optical measurement probe.

of the reactor, and two holes were drilled at the sidewall of the tube tip, from which the air was injected to the reactor in the radial direction.

Gas sampling for gas component analysis was conducted by inserting a gas sampling probe into one of the loading ports. The probe was made of stainless tube 3mm in diameter. The position of the tip end was set at the reactor centerline, and the gas was collected with this probe through a 0.3mm nozzle by connecting the tube to a vacuum-collecting chamber. The collected gas was then supplied to a gas chromatograph (Shimadzu; GC-8A) through a filtering chamber packed with silica gel, by which water and unburned methanol were removed from the gas. A component detector on the basis of TCD (Thermal Conductivity Detector) method was applied to the gas chromatography. The column (Shinwa chem.; Shincarbon ST) mounted in the chromatograph oven was calibrated for H_2, N_2, O_2, CO, and CO_2 gases. Ar gas was used as the carrier gas.

Measurements using LDV (Laser Doppler Velocimetry) were also conducted to evaluate the velocity field in the reactor. In this case, a test section different from that used in the aforementioned experiment accompanying reactions and temperature measurements was applied. An acrylic pipe of the same size as the reactor shown in Fig. 3 was made by which an optical measurement from the sidewall was available. This pipe was attached to the same evaporator and baffle plate shown in Fig. 2. The air with the flow rate equal to the total volume of the air and fuel supplied to the evaporator in the reaction experiment was provided to the upstream end of the evaporator. In the upstream of the evaporator, a particle generator (TSI; six-jet atomizer 9306) was attached and tracing particles of oil mist (DEHS: Di-Ethyl-Hexyl-Sebacate $C_{26}H_{50}O_4$, nominal diameter = 1μm) was mixed in the air. In the optical system of the LDV, the laser produced by an argon-ion laser system (Spectra Physics; model 2017L-AR) having a wavelength of 514.5nm was used together with a beam splitter coupled with a Bragg cell to detect backward flows. The Doppler burst signals from the back-scattering light of the particles were recorded and analyzed by a signal processor (DANTEC; BSA F50), which was linked to and controlled by a personal computer.

For evaluating the reforming reaction activeness, an optical probe, shown in Fig. 4, was designed to measure OH-radical chemiluminescence intensity. This probe was composed of an optical window, two plano-convex lenses, a narrow band pass filter (Edmund optics; CW = 334nm, FWHM = 10nm) and a photomultiplier (Hamamatsu; H5783-03). The optical window and each lens were made of thermal quartz glass so that OH-radical chemiluminescence light which is in ultraviolet band can penetrate through with little attenuation. The focal point of observation can be adjusted by changing the distance between two lenses ranging from 30mm to 50mm. To avoid excess heat conduction from the reactor to the optical probe, water cooling module was attached to this probe. Micro-current amplification and current-to-voltage conversion were conducted to detect weak optical signals with the photomultiplier and record them by PC via A/D converter.

The procedure applied in the reaction experiment is described in the following. The evaporator and reactor pipes were first heated by the electric band heaters so that the temperatures measured at the locations of x/D=−5.0, upstream of the baffle plate rear surface, and x/D=4.11 reached 200°C and 600°C, respectively. Then, the heaters attached to the reactor were turned off and the fuel and air were supplied to the reformer. Note that the heaters of the evaporator continued to be powered during the experiment and the temperature inside the evaporator was kept at about 200°C.

3. EXPERIMENTAL CONDITIONS

As described above, experiment was carried out with single-stage and double-stage reformers.

Table 1 shows the conditions of the experiment of the single-stage reformer. In this case, the fuel and air were both supplied to the reactor from the evaporator through the baffle plate, which means that no air was injected from the sidewall of the reactor in this case. Q_{air} and Q_{fuel} are the volume flow rates of the air and fuel fed to the evaporator, respectively. Note that Q_{fuel} represents the volume flow rate of the fuel in liquid form. ϕ_1 is the equivalence ratio based on the complete oxidative reaction. The stoichiometric ratio of the POR, therefore, is ϕ_1=3. q_e is the output power of the electric heater attached to the evaporator. As shown in Table 1, Q_{fuel} was changed under four conditions, and for each Q_{fuel}, Q_{air} was varied in the range of equivalence ratios, $3.0 \leq \phi_1 \leq 7.0$.

In Table 2, the conditions of the experiment carried out for the double-stage reformer is shown. In this case, additional air was fed to the reactor at the location between the two tube bundles, x/D=4.11. The experiment was conducted under three conditions of Q_{fuel}. In regard to each Q_{fuel}, air was supplied to the evaporator and reactor at the mass flow rates of Q_{air1} and Q_{air2}, respectively. The total amount of air provided to the reactor, $Q_{total}=Q_{air1}+Q_{air2}$, was kept constant in each Q_{fuel} case, and the ratio of Q_{air2} to Q_{air1} ($\gamma=Q_{air2}/Q_{air1}$) was changed. Therefore, the equivalence ratio at the first stage, to which fuel and air were supplied from the baffle plate, was varied in the range of $4.5 \leq \phi_1 \leq 7.0$. Note that the total equivalence ratio of the whole reformer, ϕ_{total}, calculated from the values of Q_{total} and Q_{fuel}, was kept at 4.0.

4. RESULTS AND DISCUSSION

Before moving on to the discussion, several parameters used for evaluating the performance of reformer are introduced here.

Table 1. Flow rate conditions in singe-stage case.

case	Q_{fuel} [cm^3/s]	ϕ_1	q_e [W]
ss_f1	0.066	3.0, 3.5, 4.0, 4.5, 5.0, 5.5, 6.0, 6.5, 7.0	112
ss_f2	0.092		151
ss_f3	0.122		201
ss_f4	0.145		270

Table 2. Flow rate conditions in double-stage case.

case	Q_{fuel} [cm^3/s]	ϕ_{total}	ϕ_1
ds_f1	0.066	4.0	(4.0), 4.5, 5.0, 5.5, 6.0, 6.5, 7.0
ds_f2	0.092		
ds_f4	0.145		

$\gamma=Q_{air2}/Q_{air1}$	q_e [W]
(0.0), 0.125,0.25,0.375, 0.50, 0.625, 0.75	112
	151
	270

In the present study, the quantity of the consumed methanol cannot be measured directly due to the properties of the column applied to the gas chromatograph and the silica gel chamber, which collects water and unreacted methanol. Therefore, these quantities were estimated from the concentrations of the other gases included in the exhaust gas.

Since the summation of the concentrations of H_2, N_2, O_2, CO and CO_2 in the exhaust gas was 100±2%, the major components of the gas was expected to be these five species plus water and unreacted methanol that were collected by the silica gel chamber. When paying attention on the carbon atoms, the components possessing carbon atoms among the products were found to be CO, CO_2 and unreacted methanol. Therefore, the quantity of the reacted methanol can be calculated using the concentrations of CO and CO_2 in the exhaust gas. Therefore, the methanol conversion ratio, α, is defined as follows:

$$\alpha \equiv \frac{M_{CH_3OH,\,consumed}}{M_{CH_3OH,\,supplied}} = \frac{M_{CO}+M_{CO_2}}{M_{CH_3OH,\,supplied}} = \frac{Y_{CO}+Y_{CO_2}}{Y_{N_2}} \times \frac{M_{N_2}}{M_{CH_3OH,\,supplied}} \tag{1}$$

where M_X is the molar flow rate of the X component in the exhaust gas, and Y_X is the X's concentration.

To evaluate the production efficiency of each component, the production rate of component X against 1mol of methanol supplied, ξ_X, is defined as follows:

$$\xi_X \equiv \frac{M_X}{M_{fuel,\,supplied}} = \frac{(Y_X / Y_{N_2})M_{N_2}}{M_{fuel,\,supplied}} \tag{2}$$

In calculating the production rate of H_2O, ξ_{H2O}, it is assumed that all hydrogen atoms originated from the reacted methanol are used in producing H_2 and H_2O. Thus, ξ_{H2O} can be obtained by the following equation:

$$\xi_{H_2O} = 2\alpha - \xi_{H_2} \tag{3}$$

4.1 Single-stage reformer

Figure 5 shows the streamwise temperature distributions along the centerline of the reactor in cases ss_f1~ss_f4. In Fig. 5(a), the temperature at x/D=4.11 takes

its maximum value in the case of ϕ_1=3.0 and the maximum temperature decreases as ϕ_1 increases. The same trend for temperature distribution can be seen in the other locations or in the other fuel flow rate cases. This is due to the fact that when ϕ_1 becomes small, the oxygen supply rate to the methanol increases that results in promotion of the exothermic reaction of oxidation and increase of the temperature of the reforming gas.

The streamwise temperature distributions show the similar characteristic in all cases, i.e., a maximum peak of temperature is obtained at the location of *x/D*=4.11 and the temperature level falls down in the downstream region. Therefore, it is presumed that most of the exothermic reactions take place at the area of stainless tube bundles.

Cross-sectional temperature distributions were also measured by traversing the thermocouple probe in radial direction. Figure 6 shows the results obtained in case ss_f2 of ϕ_1=5.0. The streamwise locations of measurement were *x/D*=2.32, 4.11 and 5.89 that correspond to the inlet of the first tube bundle, the middle point between two tube bundles, and the outlet of the second tube bundle, respectively. Figure 7 shows the spanwise distributions of the streamwise velocity at *x/D*=1.25, 1.62, 1.96 and 2.32, located in the area between the baffle plate and the first stainless tube bundle, obtained by the LDV measurements. Figure 7(a) and (b) shows the results of the plane crossing the center and surrounding holes of the baffle plate ((a) cross-section A-A'; see Fig. 3), and the plane crossing the middle of the surrounding holes ((b) cross-section B-B'), respectively.

In Fig. 6, at the position of *x/D*=2.32, corresponding to the inlet of the first tube bundle, the minimum peak of the temperature is observed at the centerline, and higher temperature near the sidewall. In Fig. 7(a), two peaks of *U* are observed at the locations of *r/D*=0 and 2.85. In Fig. 7(b), a maximum peak is obtained at *r/D*=0. These peak locations correspond to the areas in the downstream of the center and surrounding jets. Since the center nozzle has a larger diameter than the surrounding ones, a jet of large flow rate is issued through the center nozzle. The lower temperature obtained at the centerline is, therefore, attributed to this center jet blowing the premixed fuel gas produced from the evaporator. On the contrary, the reactor wall temperature is increased by the heat generated in the downstream of the reactor. The gas near the wall is, hence, heated and a higher temperature is obtained compared with the gas near the centerline.

As shown in Fig. 7(a), the surrounding jets convect in the downstream, and their velocity decreases as *x/D* increases. Near sidewall, flow with negative velocity is observed in Fig. 7(b). These results indicate that a flow of three-dimensional structure was generated in the downstream area of the baffle plate, and a circulation can be generated near the sidewalls due to the interaction between the center jet and surrounding jets. Consequently, most of the premixed fuel gas enters the inlet of the first tube bundle in the area near the reactor centerline.

On the other hand, at the outlet of the tube bundles, i.e., *x/D*=4.11 and 5.89 shown in Fig. 6, the temperature takes a maximum peak at the reformer centerline and decreases along the radical direction. The temperature increase obtained between *x/D*=2.32 and *x/D*=4.11 implies that the reaction mainly starts not in the area between the baffle plate and the first tube bundle, but inside the first tube bundle. Furthermore, since the maximum peaks of *U* at *x/D*=2.32 and *T* at *x/D*=4.11 are located at the centerline,

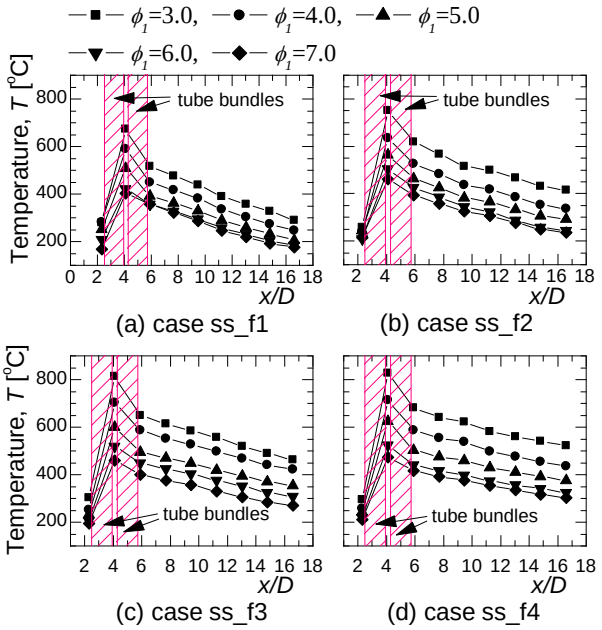

Fig. 5. Streamwise temperature distributions along reactor centerline (case ss_f1~f4).

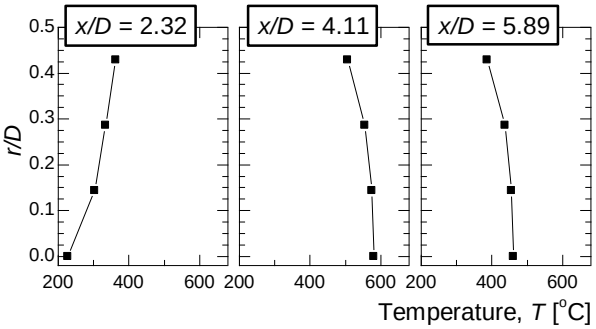

Fig. 6. Radial temperature distributions in the reactor at *x/D*=2.32, 4.11 and 5.89 (case ss_f2, ϕ_1=5.0).

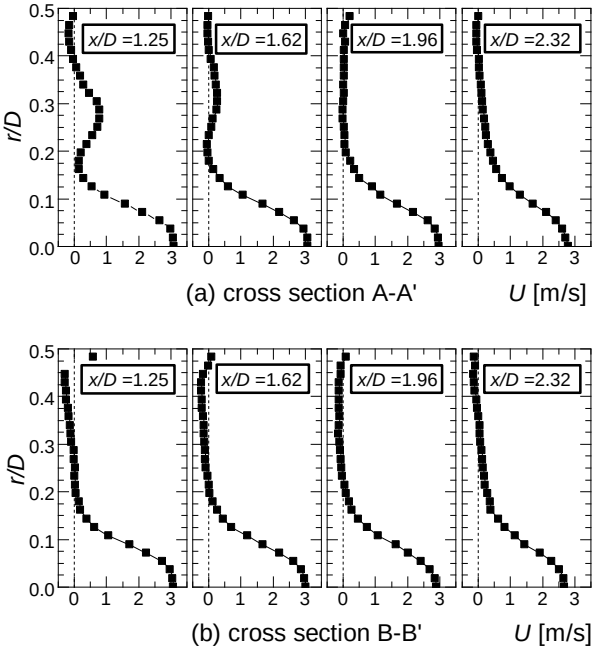

Fig. 7. Cross-sectional distributions of the streamwise velocity in the downstream area of the baffle plate (identical flow condition with case ss_f1, ϕ_1=5.0).

the reaction is expected to occur in this area.

In the present study, chemiluminescence intensity was measured by the optical probe, as explained in the previous section, for three conditions of single-stage case (equivalence ratios ϕ_1=3.0, 4.0 and 5.0). Measurement points were x/D=2.32, 4.11 and 5.89, all of which were situated on the central axis of the reactor. Among these positions, signal was strong enough to detect by the photomultiplier only at x/D=4.11. Figure 8 shows the time histories of observed voltage intensity for each equivalence ratio, ϕ_1=3.0, 4.0 and 5.0. In this figure, the corresponding OH-radical chemiluminescence intensity is shown, monitored for 600 seconds after the temperature inside the reactor became steady state. A maximum value of voltage was recorded for equivalence ratio ϕ_1=3.0 at x/D=4.11. ϕ_1=3.0 indicates the stoichiometric mixture of POR and the minimum equivalence ratio in the present study. For ϕ_1=4.0, lower voltage was observed compared to ϕ_1=3.0 at the same position. For ϕ_1=5.0, voltage output was too small to be observed. Therefore, lower equivalence ratio resulted in stronger luminescence intensity among these ϕ_1 conditions. This can be explained by the following reaction [9]:

$$CH_3OH + M \rightarrow CH_3 + OH \quad \Delta H_{R,D}=386.0\text{kJ/mol} \qquad (3)$$

Held and Dryer [9] proposed that this reaction predominates, accounting for 75% to 90% of the total decomposition reaction of methanol. Since this reaction is endothermic reaction, it is presumed that OH-radical produced through this reaction is sensitive to the gas temperature. As mentioned before, gas temperature increases in accordance with the decrease of equivalence ratio ϕ_1. Namely, the increase of ϕ_1 resulted in the decrease of exothermic heat per volume, which caused smaller methanol decomposition ratio and lower OH-radical luminescence.

Figure 9 shows the relation between the concentrations of components in the exhaust gas and equivalence ratio, ϕ_1. The concentration of O_2 is less than 0.2% in all cases indicating that the supplied O_2 were totally consumed in the reaction. The concentration of H_2 increases as ϕ_1 increases in the region of ϕ_1<5.0. However, in ϕ_1>5.0, Y_{H2} is almost constant or, in some cases, slightly decreases as ϕ_1 increases. The aforementioned gas concentrations are the values directly obtained from the gas component analysis of the exhaust gas. Therefore, effects of unburnt methanol and water removed from the gas are not sufficiently considered. In the following discussion, the trends of parameters α and ξ_X described in Eqs. (1) and (2) are discussed.

Figure 10 shows how ϕ_1 affects the conversion ratio of methanol, α. α decreases linearly as ϕ_1 increases. When ϕ_1 is small, larger reaction heat is released due to the increase of the supplied O_2 rate. The temperature inside the reactor, therefore, increases as described in Fig. 5, and the decomposition and fully-oxidation reactions of methanol become more active. On the contrary, under larger ϕ_1 conditions, the air flow rate is reduced, which incurs a fuel-rich condition in the reactions including POR and larger heat loss at the reactor wall.

The production ratio, ξ_X, is shown in Fig. 11. In the region of ϕ_1<5.0, ξ_{H2} slightly increases as ϕ_1 increases, and decreases in the region of ϕ_1>5.0. Hence, the maximum production ratio of H_2 is obtained approximately under the condition of 4.0< ϕ_1<5.0. When ϕ_1 is small, a large conversion ratio, α, is obtained as shown in Fig. 10. However, oxidization of H_2 to H_2O also becomes active due to the high

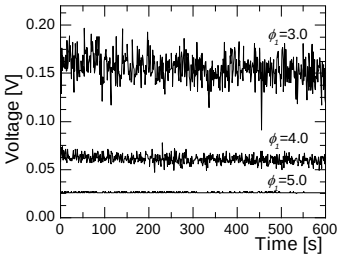

Fig. 8. OH-radical chemiluminescence intensity for the cases of equivalence ratios ϕ_1=3.0, 4.0 and 5.0.

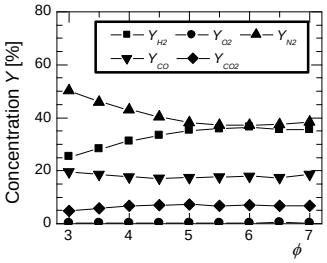

Fig. 9. Relation between gas concentration and equivalence ratio (case ss_f4).

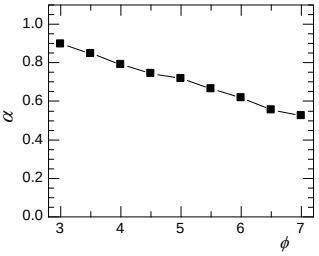

Fig. 10. Methanol conversion ratio (case ss_f4).

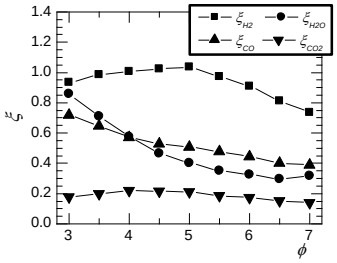

Fig. 11. Mole production rates (case ss_f4).

temperature which leads the concentration of H_2 to decrease as shown in Fig. 9. On the contrary, under larger ϕ_1 condition, the conversion ratio of methanol becomes small. Thus, a trade-off matter exists between α and Y_{H2}. This is believed to be the reason why the maximum peak of ξ_{H2} is obtained at 4.0< ϕ_1<5.0

To integrate all the results obtained through the temperature, velocity and chemiluminescence measurements, it is presumed that the reforming reactions start in the first stainless tube bundle, and the most of the reactions take place upstream of the end of the second tube bundle. Furthermore, the temperature takes its maximum value at the centerline of the reactor, which means intensive reaction takes place at the center region of the reactor.

Based on these results mentioned above, it is effective to supply the secondary air at the position of x/D=4.11, where the primary important reforming reaction seems active.

4.2 Double-stage Reformer

Figure 12 shows the streamwise distributions of the temperature along the reactor centerline obtained in the cases of double-stage reformer. The results of case ss_f4 of ϕ_1=4.0 are included in the figure for comparison. The parameter γ is defined as the ratio of the air flow rate supplied to the second and first stages.

At x/D=4.11, the temperature decreases as γ increases. In the downstream area (x/D≥6), on the contrary, the temperature increases as γ increases. Since the total amount of air supplied to the reactor in cases ds_f1, ds_f2 and ds_f4 was fixed at the constant value corresponding to case ss_f4, an increase of γ implies the increases of ϕ_1 and air flow rate supplied to the second stage. In the double-stage reformer, the air and fuel were supplied to the first stage in the same way as in the single-stage case, and a common reaction characteristic was expected to take place. The gas temperature was, therefore, reduced under larger ϕ_1 condition due to the fuel rich condition obtained in the first stage of the reactor as mentioned in the previous section.

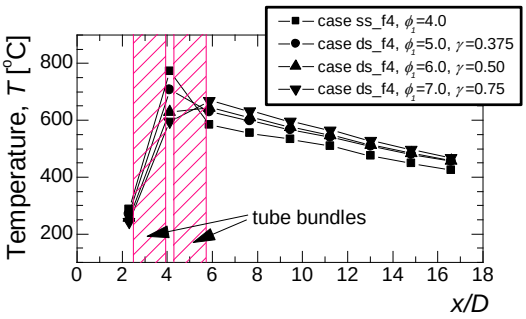

Fig. 12. Streamwise temperature distributions (comparison of cases ss_f4 and ds_f4, ϕ_{total}=4.0).

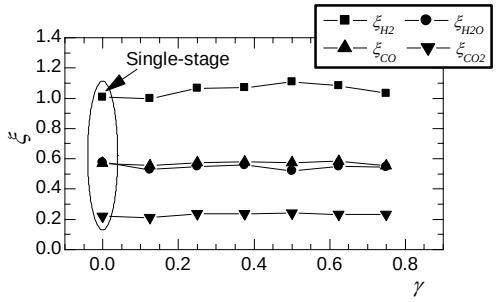

Fig. 13. Relation between γ and ξ_X (case ds_f4).

On the other hand, as indicated in Fig. 10, larger amount of unreacted methanol enters the second stage in association with the increase of ϕ_1. In combination with the additional air injected to the second stage, a more active reaction, therefore, takes place in the downstream. This is believed to be the main reason why a higher temperature is obtained in case ds_f4 in the downstream area.

Figure 13 illustrates how γ affects ξ_X. The results of the single-stage case are included in the figure for comparison. In case ds_f4, a slight increase of ξ_{H2} is observed as γ increases in the area of $0.2 \leq \gamma \leq 0.6$, and the maximum difference between the results in cases ss_f4 and ds_f4 is approximately 10%. This implies that the production ratio of H_2 is not largely affected by increasing the reformer stage from single- to double-stage; at least the performance of double-stage case is not inferior to that of the single-stage case in the present study.

Although a noticeable improvement was not achieved, in terms of the reaction efficiency, by introducing the double-stage reforming, the results obtained in Figs. 12 and 13 indicate the possibility of controlling the temperature of the reformer by multiplying the reaction stages without incurring a serious deterioration of the reforming efficiency. This is important since the reformer can be protected from thermal fatigue by applying an appropriate gas supply ratio and preventing the generation of a significant increase of local temperature.

5. CONCLUSIONS

In the present article, single- and double-stage methanol fuel reformer was experimentally evaluated particularly on the basis of the thermal and reaction characteristics. The major conclusions obtained are listed in the following.

1. A multistage reformer consisting of evaporator and reactor was fabricated and operated under the conditions of varying the equivalence ratio, ϕ_1, in the range of $3.0 \leq \phi_1 \leq 7.0$. Hydrogen production and a suitable temperature level for practical use were obtained by the reformer.
2. A better performance was obtained under the conditions of ϕ_1=4.5~5.0 than under the stoichiometric value of partial oxidation, ϕ_1=3, in the present reformer.
3. An optical measurement in the reformer was conducted and the correlation between OH-radical chemiluminescence intensity and the gas temperature condition was confirmed.
4. A maximum peak existed in the H_2 production rate per supplied fuel in relation with ϕ_1. This is due to the trade-off between the methanol conversion ratio, α, and H_2 concentration.
5. In the double-stage case, temperature control of the reformer was possible without deteriorating the reforming efficiency. Moreover, in some cases, increase of the H_2 production rate by 10% was obtained in this case compared with the singe-stage case.

6. REFERENCES

1. A. L. Dicks, Hydrogen Generation from Natural Gas for the Fuel Cell Systems of Tomorrow, J. Power Sources, 61 (1996), pp. 113-124.
2. H. Marsh and D. Thingarajan, AIChE Ammonia Safety Symposium, (1992).
3. M. Dunster and J. Korchnak, Production of Synthesis gas from Hydrocarbonaceous Feedstock, Eur Patent No. 303438, (1989).
4. T. Calcott and T. Deague, US Patent No. 4 042 344, (1977).
5. K. Tatsumi, K. Kuwabara, Y. Rai and K. Nakabe, Heat and Reaction Characteristics of Multistage Alcoholic-Fuel Reformer, Proc. 18th Int'l Symp. Transport Phenomena (ISTP-18), (2007), pp. 847-854.
6. J. Larminie and A. Dickes, Fuel Cell Systems Explained, John Wiley & Sons Inc. (2003).
7. B. Li, S. Kado and Y. Mukainakano, Temperature Profile of Catalyst Bed during Oxidative Steam Reforming of Methane over Pt-Ni Bimetallic Catalysts, Applied Catalysis A, General 304 (2006), pp. 62-71.
8. C. Pan, R. He and Q. Li, Integration of High Temperature PEM Fuel Cells with a Methanol Reformer, J. Power Sources, 145 (2005), pp. 392-398.
9. T. J. Held and F. L. Dryer, A Comprehensive Mechanism for Methanol Oxidation, Int'l J. Chemical Kinetics, 30 (1998), pp. 805-830.

ACKNOWLEDGEMENT

This work is partially supported by the Mazda foundation, General Sekiyu K. K. research foundation, and Japan Society for the Promotion of Science. The authors would like to gratefully acknowledge their support.